

Elaboration and characterization of sulfated and unsulfated V_2O_5/TiO_2 nanotubes catalysts for chlorobenzene total oxidation

C. Gannoun^{a,*}, A. Turki^a, H. Kochkar^{a,b}, R. Delaigle^c, P. Eloy^c,
A. Ghorbel^a, E.M. Gaigneaux^c

^a Laboratoire de Chimie des Matériaux et Catalyse, Faculté des Sciences de Tunis (FST), Campus Universitaire El Manar 2092, Tunisia

^b Centre National des Recherches en Sciences des Matériaux (CNRSM), Technopôle de Borj-Cédria, Hammam-Lif 2050, Tunisia

^c Université Catholique de Louvain, Institute of Condensed Matter and Nanosciences (IMCN), Division «Solids, Molecules and ReactiviTy (MOST)», Croix du Sud 2/17, B-1348 Louvain-la-Neuve, Belgium

ARTICLE INFO

Article history:

Received 14 November 2012

Received in revised form 2 August 2013

Accepted 7 August 2013

Available online 22 August 2013

Keywords:

TiO₂ nanotubes

Sulfate

Vanadia

Chlorobenzene oxidation

ABSTRACT

This paper examines the use of TiO₂ nanotubes (HNTs) as supports for V₂O₅ based catalysts in the total oxidation of chlorobenzene. The effect of the addition of SO₄²⁻ onto the support is also discussed. Vanadium was introduced either by direct incorporation of V during the elaboration of the nanotubes (in situ elaboration), or by the impregnation of V on the surface of the supports (ex situ elaboration). The obtained catalysts have been characterized by means of ICP-AES, N₂ adsorption-desorption at 77 K, XRD, DRIFTS, XPS, H₂-TPR and NH₃-TPD. We demonstrated that sulfating step highly improves the catalytic performances of V-HNTs catalysts. This is due to an increased global acidity and a higher reactivity of redox sites thanks to the electronic interaction between sulfated titania and VO_x species. Moreover, it seems that the 'in situ' or 'ex situ' elaboration route of sulfated V-catalysts influences the environment of vanadium species. In particular, the 'in situ' route leads to a more efficient catalyst.

© 2013 Elsevier B.V. All rights reserved.

1. Introduction

Vanadia-based catalysts, such as vanadia-titania, vanadylphosphates, vanadia on silica, find widespread application in industry mainly for partial oxidation (e.g. maleic and phthalic anhydride syntheses) and for the SO₂ to SO₃ oxidation, a key step in the sulfuric acid synthesis process. Among several other research groups, the Krakow group headed by Haber performed very valuable fundamental and applied investigations concerning vanadia-based oxidation catalysts which resulted in a quite satisfactory picture of the corresponding catalytic phenomena [1]. The catalytic total oxidation of chlorobenzene has been widely studied as model reaction of dioxin combustion in waste gases treatments. Since the work of Jones and Ross [2], several research groups studied the performances of commercial and innovative vanadia containing catalysts in VOC and Cl-VOC combustion. Amiridis et al. evaluated the catalytic oxidation of dichlorobenzene over different supported metal oxides, with respect to the V₂O₅-TiO₂ system [3]. Cr₂O₃ and V₂O₅ based catalysts have shown the highest activity, which

is also affected by the nature of the support. Titania seems to be the most effective catalyst support for this application while alumina is less indicated. This observation underlines the electronic effect between titanium oxide (weak Lewis acidity) and vanadia species [4]. In fact, the surface structure of TiO₂ and Al₂O₃ are different. Al₂O₃ exhibits only Lewis acidity, while TiO₂ develops Lewis acidity as well as redox properties. Consequently, in the case of TiO₂, the redox properties of vanadium will be modified leading to an electronic interaction between this support and VO_x species. Vanadia loading is a key point for the activity and it has been suggested that a single redox surface site participates in the kinetically significant steps, with the formation of crystalline V₂O₅ being detrimental on oxidation activity [5]. The addition of WO₃, and other dopants, affects the acidic properties of the catalytic surface and it has reported recently to influence the performance of vanadia based catalyst in total oxidation of chlorobenzene [6,7]. In fact, TiO₂/WO₃ catalysts are reported to be more active than the TiO₂ materials, although increasing Brønsted acidity by WO₃ introduction increases chlorinated byproducts formation, such as chloromaleic anhydride.

The high oxidative activity of V₂O₅ supported over acidic SiO₂/WO₃/TiO₂ has been reported by Albonetti et al. [8]. Silica leads to a stabilization of the catalyst and favors formation of highly dispersed VO_x species, at least at low vanadia loadings. Lewis acidity of the catalyst surface is instead proposed to be involved in another

* Corresponding author at: Laboratoire de Chimie des Matériaux et Catalyse, Faculté des Sciences de Tunis (FST), Campus Universitaire El Manar 2092, Tunisia.
Tel.: +216 96940755.

E-mail address: gannoun.chiraz@gmail.com (C. Gannoun).

adsorption–oxidation mechanism, mainly occurring over transition metal oxide catalysts, through nucleophilic substitution of the chlorine atom to form strongly adsorbed chlorophenylate species, the oxidation of aromatic ring to give carboxylate species being a later reaction step. This mechanism has been reported for chloro-carbon oxidation over V_2O_5/TiO_2 and $V_2O_5/MoO_3/TiO_2$ catalysts [9,10].

The role of different VO_x species in total chlorobenzene oxidation has been widely discussed in several papers from our group as well as the effect of a transition metal oxide dopant [11–14]. The authors performed benzene total oxidation as screening tests over a number of transition metal based catalysts, whose formulation has been defined in order to have a theoretical coverage of active phase spreading over titania, sulfated titania, alumina, and silica supports, kept below the monolayer. Recently, we investigated a series of TiO_2 , $TiO_2-SO_4^{2-}$, TiO_2-CeO_2 and $TiO_2-SO_4^{2-}-CeO_2$ aerogel supports prepared by a sol gel route on which active vanadia was deposited via impregnation method. Catalytic tests indicated that Ce-doped V_2O_5 -based catalysts achieve 100% chlorobenzene conversion at 400 °C. This could be related to the redox properties of cerium, being in the form of CeO_2 in the prepared catalysts. Besides, sulfate containing vanadia–titania samples prepared with or without ceria had considerably improved catalytic properties in the chlorobenzene oxidation in the lower temperature range (200–300 °C) as compared to corresponding unsulfated catalysts. In fact, sulfation generates additional weak acidic sites at the catalyst surface. This likely promotes the chlorobenzene adsorption. As sulfation also improves the redox properties of both vanadium and cerium species at the surface of the catalysts, a marked increase in activity was observed. This was discussed due to the existence of strong interaction between vanadia and sulfates on the one hand, and between ceria and sulfates on the other hand. These interactions would induce a higher reactivity of redox sites leading to the observed higher efficiency of catalysts [15]. In a recent paper, we demonstrated that sulfate containing Vanadia–titania aerogel catalysts prepared via sol-gel method had also considerably improved catalytic properties in the chlorobenzene oxidation at high temperature as compared to corresponding unsulfated gels [16]. On the one hand, in all flow papers, it seems that TiO_2 surface area is a key factor for good VO_x dispersion. On the other hand, Titanates nanotubes materials have been discovered by Kasuga et al. [17,18] using a simple, reproducible and not expensive alkaline hydrothermal method. More recently, Kochkar et al. [19–21] demonstrated that hydrogenotitanate nanotubes with controlled properties (tuned morphology and diameter, high specific surface area and important cation exchange capacity) can be successfully obtained.

Motivated by the favorable characteristics of nanotubular morphology of TiO_2 in terms of specific surface area, morphology, crystallinity and porosity [19–22], we thus investigate in this study, the use of TiO_2 nanotubes as support for V_2O_5 based catalysts for the total oxidation of chlorobenzene. The effect of the addition of SO_4^{2-} onto the support will also be discussed, as acidic moieties in the formulation – in particular sulfates – have indeed been already shown to be beneficial on the performances of VO_x/TiO_2 catalysts [16,23,24].

2. Experimental

2.1. Elaboration of the catalysts

The alkaline hydrothermal method [19,21], was used to elaborate the titanate nanotubes materials (HNTs). Typically, a commercial TiO_2 (Degussa P25, 0.5 g) was dispersed in 15 mL of an aqueous solution of NaOH (11.25 M) and placed into a Teflon-lined stainless steel autoclave. The autoclave was statically heated

at 130 °C for 20 h. A white precipitate was isolated upon filtration and washed intensively with hot ultra pure water until the pH value of the supernatant had attained a value close to 9. In a second step, an aqueous suspension containing the precipitate was neutralized using a 0.1 M HCl solution until a pH value of 7 was reached. After neutralization, a second washing with 500 ml of boiling ultra pure water is carried out in order to remove the NaCl formed in excess followed by a filtration. To ensure that all Na^+ is removed, a second washing with 1 M HCl solution and 500 ml of boiling ultra pure water followed by a filtration were carried out. Finally, the support was dried at 80 °C for 24 h.

Unsulfated $V_2O_5/HNTs$ based catalyst was elaborated by impregnating HNTs with NH_4VO_3 as precursor. This sample is labeled V-HNTs. However, sulfated $V_2O_5/HNTs$ materials were prepared as follow:

- 'Ex situ' elaboration: Typically 0.5 g of HNTs materials were sulfated using 0.13 g of $(NH_4)_2SO_4$ (99.65%) according to a molar ratio $n_S/n_{Ti} = 0.2$ and corresponding to a S content of 8 wt.%, before being impregnated by 0.028 g of ammonium metavanadate (NH_4VO_3) (99.99%). The obtained material is dried at 80 °C for 24 h. This sample is labeled V-HNTs-S1.
- 'In situ' elaboration: Typically 0.028 g of ammonium vanadate (NH_4VO_3) is introduced during the elaboration stage of the nanotubes by the alkaline hydrothermal method. The obtained material is impregnated by sulfates using 0.13 g of $(NH_4)_2SO_4$ (99.65%). Finally, the material is dried at 80 °C for 24 h. This sample is labeled V-HNTs-S2.

The two kinds of catalysts (sulfated and unsulfated) contain ca 2.5 wt.% of vanadium.

The obtained materials were finally calcined at 400 °C under air flow using a ramp of 2 °C min⁻¹.

2.2. Characterization of catalysts

The elemental analysis was performed by inductively coupled plasma-atomic emission spectroscopy (ICP-AES) allowing estimating the weight percentage of S and V. Typically, 50 mg of the sample were dissolved in concentrated acidic solution containing 2/3 HCl and 1/3 HNO₃. Finally, the obtained solution was diluted in 100 ml of ultrapure water before being analyzed by ICP-AES. The measurements were performed on a Horiba Jobin Yvon apparatus, Model Activa.

Specific surface area and pore volume measurements of the samples were done by N₂ physisorption at 77 K using a Micromeritics ASAP 2020 apparatus. Prior to N₂ physisorption, the samples were outgassed in vacuum during 6 h at 200 °C.

X-ray diffraction patterns (XRD) were obtained using a MRD PRO PANalytical X'Pert PRO instrument with Cu K α radiation ($\lambda = 1.5418 \text{ \AA}$) at the rate of 0.02°/s from 5° to 70°.

In situ diffuse reflectance infrared spectroscopy (DRIFTS) spectra were recorded on a Bruker IFS 55 spectrophotometer equipped with a Thermo Spectra Tech reacting cell at a spectral resolution of 4 cm⁻¹ and accumulating 200 scans. Samples were treated 'in situ' under a helium flow (30 cm³ min⁻¹) at 500 °C.

Total acidity was evaluated by temperature-programmed desorption of ammonia (TPD/NH₃) using a quadrupole Balzers QMC 311. Before NH₃ desorption, the samples were pre-treated under He flow (60 ml min⁻¹) at 200 °C for 1 h. NH₃ adsorption was performed under ambient conditions by flowing 0.5% NH₃ in He over the catalyst until saturation and then following the desorption of NH₃ along a temperature-programmed treatment under He from 50 to 500 °C using a heating rate of 10 °C min⁻¹.

Temperature programmed reduction (TPR) experiments were performed in a dynamic apparatus using 5% H₂ in helium flowing at

Table 1

Element analysis and nominal composition of V-HNTs, V-HNTs-S1 and V-HNTs-S2 calcined at 400 °C.

Catalyst	Bulk composition (wt.%)		Nominal composition (wt.%)	
	V	S	V	S
V-HNTs	2.3	–	2.5	–
V-HNTs-S1	2.4	3.69	2.5	8
V-HNTs-S2	2.3	4.01	2.5	8

60 ml min⁻¹. Experiments were carried out in the range 30–800 °C. The inlet and outlet gas compositions were measured using a quadrupole mass spectrometer QMC 311 Balzers coupled to the reactor.

X-ray photoelectron spectra (XPS) were collected on a SSI X probe spectrometer (model SSI 100, Surface Science Laboratories, Mountain View, CA, USA) equipped with a monochromatized AlK_α radiation (1486 eV). The samples powders, pressed in small stainless steel troughs of 4 mm diameter, were placed on an insulating homemade ceramic carousel. The pressure in the analysis chamber was around 10⁻⁶ Pa. The angle between the surface normal and the axis of the analyser lens was 55°. The analyzed area was approximately 1.4 mm² and the pass energy was set at 150 eV. The C1s peak of carbon has been fixed to 284.8 eV to set the binding energy scale. Data treatment was performed with the CasaXPS program (Casa Software Ltd., UK) and some spectra were decomposed with the least squares fitting routine provided by the software with a Gaussian/Lorentzian (85/15) product function and after subtraction of a non linear baseline.

2.3. Catalytic test

Catalytic tests were performed with 200 mg of catalyst (200–315 µm) diluted in 800 mg of inactive glass spheres with diameters in the range 315–500 µm in a metallic fixed-bed micro-reactor (PID Eng&Tech, Madrid, Spain) operating at atmospheric pressure and fully monitored by computer. The gas stream was composed of 100 ppm of chlorobenzene, 20 vol.% of O₂ and helium as diluting gas to obtain 200 ml min⁻¹ (space velocity (VVH)=37,000 h⁻¹). The reaction was run from 100 to 400 °C in a step mode with a 150 min plateau at each temperature investigated. Analysis of reactants and products was continuously performed by on line gas chromatography (GC).

3. Results and discussion

Nominal and experimental chemical compositions of the investigated samples are compared in Table 1. The results indicate that vanadium was successfully incorporated in V-HNTs catalyst. The small difference observed may result from inaccuracies in the preparation of the solution of sample for ICP analysis (ca. weighing). For sulfated samples, differences between the theoretical and the experimental sulfur content could be attributed to the loss of some of the sulfur during thermal post-treatment [16].

The nitrogen adsorption–desorption isotherms of the HNTs, V-HNTs, V-HNTs-S1 and V-HNTs-S2 samples (Fig. 1) present a type IV profile with H3 hysteresis loops characteristic of non-rigid aggregates of particles giving rise to slit-shaped pores. This reveals that the hydrothermal treatment of the non-porous TiO₂ P25 leads to the formation of developed textural properties. The textural properties of the samples are summarized in Table 2. First, the surface area of HNTs sample (174 m² g⁻¹) decreases after impregnation with vanadium (103 m² g⁻¹) indicating a partial blocking of small pores by VO_x species. However, the average pore diameter increases by a factor of 1.6. While the V-HNTs sample presents a

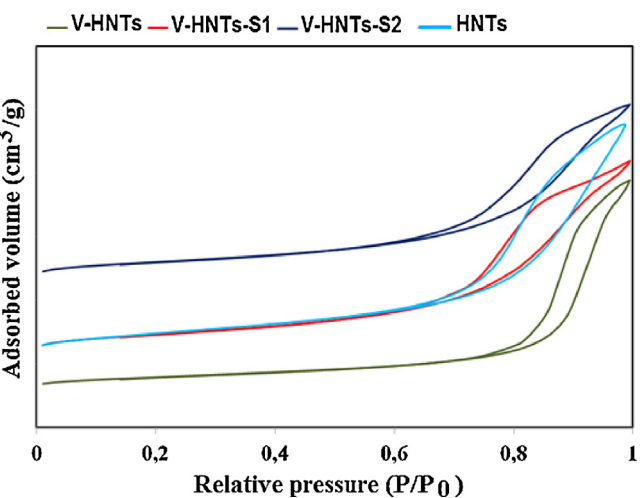


Fig. 1. N₂ Adsorption–desorption isotherms at 77 K of the V-HNTs, V-HNTs-S1 and V-HNTs-S2 samples treated at 400 °C.

Table 2

Textural properties of sulfated and unsulfated catalysts calcined at 400 °C.

Catalyst	S _{BET} (m ² g ⁻¹)	Pore diameter (nm)
HNTs	174	106
V-HNTs	103	17.1
V-HNTs-S1	144	10.8
V-HNTs-S2	138	11.5

pore distribution with a maximum at a diameter of 17.1 nm, the V-HNTs-S1 and V-HNTs-S2 samples show a maximum pore size value at 10.8 and 11.5 nm (Fig. 2). The presence of sulfates in the catalysts leads to clear changes in the textural properties. These results could be attributed to the reorganization of TiO₂ crystallites sizes after sulfation step. Finally, all catalysts are mesoporous with surface areas in the range of 100–144 m² g⁻¹ which is an adequate range for VOCs catalytic abatement.

The XRD patterns of the catalysts are shown in Fig. 3. The assignment of the structure of titanate nanotubular materials was the subject of intense controversy. In its initial study, Kasuga et al. [17] characterized their product as anatase. This assumption was confirmed in a more recent paper [25]. On the contrary, on the basis of XRD, selected-area electron diffraction (SAED) and

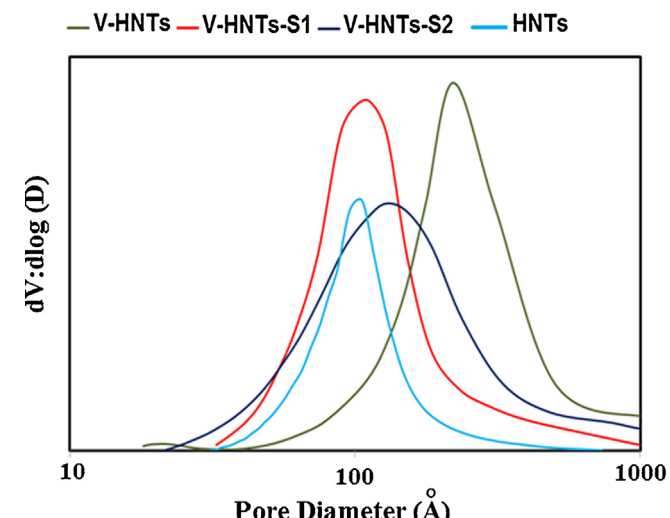


Fig. 2. Porous distributions of HNTs, V-HNTs, V-HNTs-S1 and V-HNTs-S2 materials treated at 400 °C.

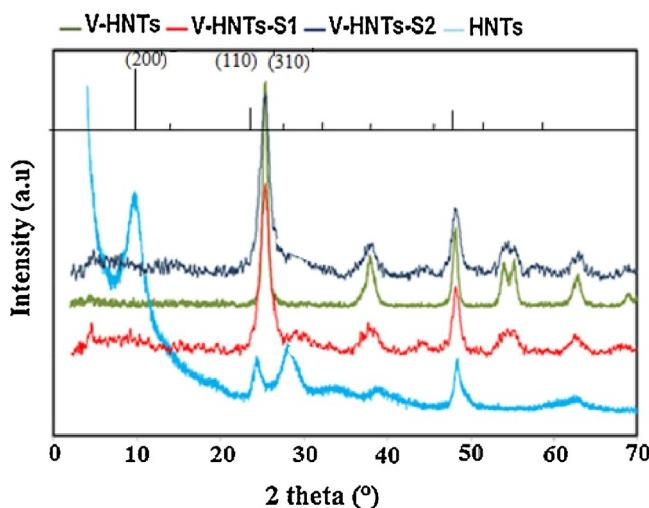


Fig. 3. X-ray powder diffraction patterns of HNTs, V-HNTs, V-HNTs-S1 and V-HNTs-S2 samples treated at 400 °C.

high-resolution transmission electron microscopy (HRTEM) data, Peng et al. [26,27] proposed that the crystal structure of titanate nanotubes corresponds to the layered trititanic acid ($H_2Ti_3O_7$) with a monoclinic crystal structure. On the basis of XRD and transmission electron microscopy (TEM) data, Nakahira et al. [28] assigned HNTs produced using alkaline hydrothermal treatment to a tetratitanic acid, $H_2Ti_4O_4(HO)_2$. On the basis of studies of the sodium content of titanate nanotubes at various pH values, during acid washing (in combination with XRD and TEM data), Yang et al. [29] and Kochkar et al. [19] proposed the following crystal structure of titanate nanotubes: $H_2Ti_2O_5 \cdot H_2O$ with an orthorhombic unit cell. In conclusion, nanotubes are assumed to be layered protonated polytitanates ($H_{2-x}M_xTi_nO_{2n+1}$ with $M = Na$ or K ; $x \leq 2$; $n = 2, 3, 4$ or 5) and sodium can be exchanged under acidic medium.

Our results revealed that the V-HNTs catalyst is very well crystallized and only anatase phase is detected (diffraction peaks at $2\theta = 25^\circ, 37^\circ, 48^\circ$ and 53° (PDF-ICDD 21-1272)). However, for the sulfated catalysts, a typical XRD pattern of anatase and several weak peaks of HNTs support are observed. Pure HNTs samples indeed present broad diffraction peaks mainly at 2θ values of $10.0^\circ, 24.6^\circ, 28.4^\circ$, and 48.5° which can be ascribed neither to anatase nor to rutile. These XRD patterns correspond to orthorhombic phase of the type $H_2Ti_2O_5 \cdot H_2O$ (or $Na_xH_{2-x}Ti_2O_5 \cdot H_2O$ for Na-HNTs) [19,30–33]. Complementary Rietveld analysis of this sample excludes the possibility of formation of a $H_2Ti_3O_7$ orthorhombic phase as reported by other studies [34–36]. The (200) peak at $2\theta = 10.0^\circ$ corresponds to the interlayer distance between walls of the nanotubes [30,37]. These results suggest that sulfate groups do not destroy the nanotubular morphology. Moreover, no vanadia patterns were observed in any of the elaborated catalysts indicating that V_2O_5 nanoparticles are (i) well dispersed onto the surface of the supports or (ii) having very small particle size.

Recently, we studied the structural, textural and morphological stability of HNTs support (with sodium or sodium free samples) as a function of the calcination temperatures [38]. The complete removal of sodium from the titanate orthorhombic structure did not modify substantially the morphology of the TiO_2 material. HNTs is still composed of homogeneous bundles of nanotubes with a diameter of 10–14 nm and a wall thickness of 2–3 nm. However, some modifications can also be noticed. After calcination at 400 °C for 2 h, the HNTs-400 sample still presents nanotubular morphology. HNTs-400 forms assembly of aggregated nanotubes resulting in the formation of an inter-granular porosity in the voids formed between aggregated tubes. HRTEM image of the extremity of one

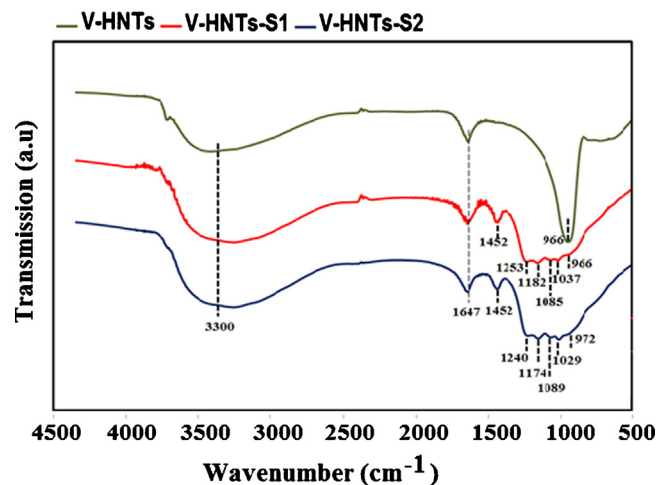


Fig. 4. DRIFTS spectra of V-HNTs, V-HNTs-S1 and V-HNTs-S2 samples treated at 400 °C.

of these nanotubes showed that this sample presents open ends with an outer diameter of about 10 nm, an inner diameter of 4 nm and a length of about 100–300 nm. The lattice fringes are more clearly discernable after calcination at 400 °C suggesting a higher crystallinity. An interlayer d spacing of 0.34 nm can be measured corresponding to the (101) plane of anatase suggesting that the orthorhombic phase relative to titanate nanotubes was already transformed into anatase at this temperature of calcination. After calcination at 500 °C, the HNTs-500 sample has completely lost its monodimensional morphology leading to the formation of plate-like particles. A d spacing of 0.36 nm can still be measured showing that (101) planes of anatase can still be detected even after collapse of the nanotubular morphology. After calcination at 600 °C, only agglomerated spherical particles without any precise morphology are obtained. Noticeably, rod-like objects are not observed. Statistical distributions of the average size of particles obtained on HNTs-500 and HNTs-600 showed a progressive increase in size of the TiO_2 particles due to a sintering phenomenon. In conclusion, our catalysts are stable (in terms of structural and morphological properties) in the range of the reaction temperatures (100–400 °C).

The DRIFTS spectra of the prepared catalysts treated at 400 °C are given in Fig. 4. All samples exhibit bands at 3300 and 1647 cm^{-1} assigned to stretching vibrations of O–H and bending vibrations of molecular water, respectively, were observed for all samples. These results suggest the presence of certain number of surface hydroxyl groups. In addition, three bands appeared at 1452, 1182, and 1085 cm^{-1} ; the first band was assigned to the asymmetric stretching mode of SO in covalent sulfate species $(TiO_2)SO_2$ [39,40], while the latter two originated from surface vibrations incorporating water molecules causing deformation of the surface TiO_2 octahedra surrounding surface Ti atoms [41]. A band in the range of 960–975 cm^{-1} and centered at 966 cm^{-1} is probably characteristic of Ti–O–Ti anatase structure or due to vanadate species in the interlayer spaces. The sharp band at 1030 cm^{-1} encountered in the case of sulfated materials could be assigned either to the V=O stretching vibration mode of crystalline V_2O_5 [42] or to the vibration modes of sulfate species [39,40].

In addition, as shown in Fig. 4, there are three peaks at 1452, 1253 and 1085 cm^{-1} matching the bidentate symmetry [43]. Its configuration could be chelating bidentate or bridged bidentate (Fig. 5).

Based on the isotope exchange and IR results, Saur et al. [44] suggested that the structure of the sulfated oxide under dry conditions is $(Ti-O)_3S=O$, whereas under wet conditions, the surface structure is the bridged bidentate form with H forming a Brønsted

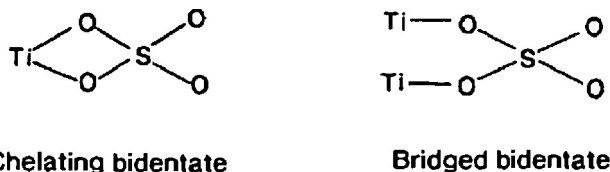


Fig. 5. Schematic suggestion of the electronic interaction titanium-sulfates.

site (Ti_2SO_4)H. Moreover, the absence of peak at 1201 cm^{-1} characteristic of the chelating bidentate symmetry [42] proves that, in our study, we have more likely the bridged configuration. Therefore, from the symmetry analysis of the DRIFTS spectra, the reaction conditions (with water) and the isotope IR spectra of Saur et al. [44], it's concluded that the sulfated vanadia-titania is bridged bidentate with titania whatever the method used for the vanadium incorporation. Fig. 6 suggests that a strong interaction could occur between vanadia, titania, and sulfate species.

We investigated the surface composition of the V-HNTs catalysts using XPS measurements. The binding energy values of the elements O1s, Ti 2p, S 2p and V 2p and the surface atomic ratios V/Ti, S/Ti are displayed in Table 3. The binding energies of Ti 2p_{3/2} for all catalysts were around 459 eV, characteristic of Ti^{4+} in TiO_2 [45,46]. A contribution with binding energies around 515 and 517 eV was detected for all samples suggesting that vanadium, in this study, was present as a mixture of IV and V oxidation states [47,48]. The XPS binding energies of the O1s were around 530 eV, which is typical of oxide oxygen [49,50]. For sulfated catalysts, a peak with a binding energy near 169 eV was measured for the S 2p_{3/2}. According to literature, such an XPS band represents the existence of sulfate on the catalyst surface [51,52]. The surface atomic ratios V/Ti are quiet similar for both V-HNTs and V-HNTs-S1 samples. However, in V-HNTs-S2 sample obtained by 'in situ' elaboration, the V/Ti ratio diminishes to 0.049 revealing a decrease of the relative exposure of vanadium at the surface of this catalyst. Furthermore, sulfate ions are exposed similarly in both sulfated samples.

In order to determine how the sulfate concentration impacts the surface acidity on V-HNTs catalysts, the acidity behavior of V-HNTs, V-HNTs-S1 and V-HNTs-S2 catalysts were evaluated by NH₃-TPD experiments. The obtained profiles are given in Fig. 7. The NH₃ desorption profile of the V-HNTs sample shows two unresolved peaks at around 100 and 380 °C which could be attributed to NH₃ desorbing from weak and strong acidic sites, respectively [53,54]. The presence of sulfates significantly enhances the total acidity of the HNTs materials. Especially, sulfate groups interact with titanium species, creating more numerous weak and strong

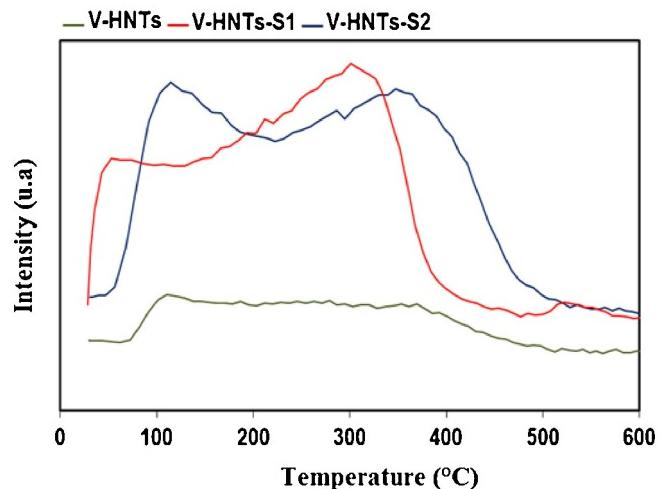


Fig. 7. NH₃-TPD profiles of V-HNTs, V-HNTs-S1 and V-HNTs-S2 samples treated at 400 °C.

acidic sites as indicated by the increase of the intensities of the two peaks mentioned above. This enhancement is highly beneficial for the catalytic performances of V_2O_5/TiO_2 catalysts as discussed in earlier works [12,16,45]. In fact, the weak acidic sites would promote the adsorption of the chlorobenzene on the support while strong acidic sites would improve the spreading of the V_2O_5 species. Moreover, it seems that the strength of acid sites is influenced by the elaboration route of the catalysts namely: 'in situ' or 'ex situ'. In fact, the NH₃-desorption temperatures from weak and strong acid sites are shifted toward lower temperatures in the case of V-HNTs-S1 reflecting a decrease in the strength of the acid sites. However, the strong acidity observed in the case of V-HNTs-S2 is likely related to the lower vanadium exposure as demonstrated by XPS and to the lower agglomeration of vanadium species.

The reducibility of sulfate and vanadium was examined by means of H₂-TPR (Fig. 8). A reference TPR profile was measured for a sulfated support (HNTs-S) elaborated with a molar ratio S/Ti = 0.2 following the synthesis described in Section 2. HNTs-S exhibits two peaks around 679 and 665 °C which could be assigned to the reduction of sulfate species into SO₂ essentially as observed in earlier works [55–57]. For V-HNTs catalyst, a weak peak centered at about 454 °C might be ascribed to the reduction of VO_x species [58,59]. The addition of SO₄²⁻ is observed to slightly inhibit the reduction

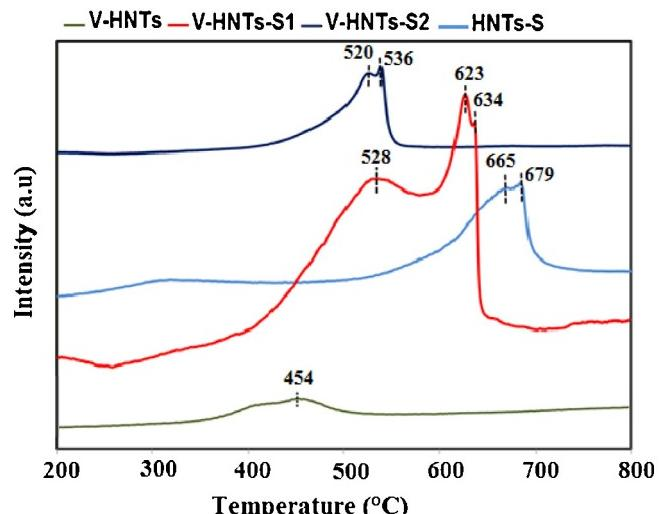


Fig. 8. H₂-TPR profiles of V-HNTs, V-HNTs-S1 and V-HNTs-S2 samples treated at 400 °C.

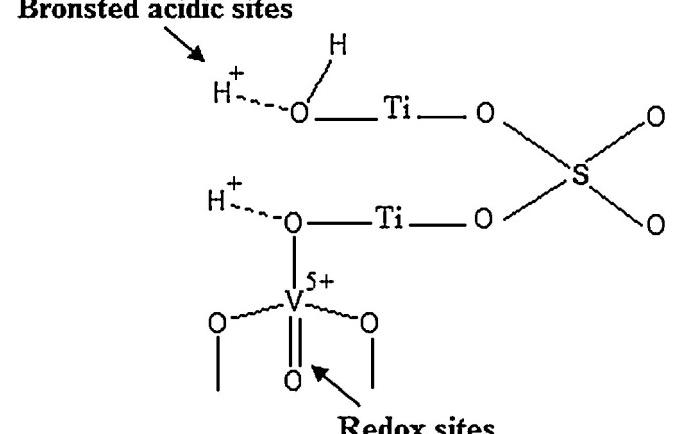


Fig. 6. Schematic suggestion of the electronic interaction vanadium-titanium-sulfates.

Table 3

XPS binding energies of V-HNTs, V-HNTs-S1 and V-HNTs-S2 catalysts calcined at 400 °C.

Catalyst	Binding energy (eV)					Atomic ratio	
	O1s	Ti 2p _{3/2}	V 2p _{3/2} ⁵⁺	V 2p _{3/2} ⁴⁺	S 2p _{3/2}	V/Ti	S/Ti
V-HNTs	529.9	458.6	517.3	515.8	—	0.086	
V-HNTs-S1	530.1	458.9	517.1	515.9	169.1	0.081	0.318
V-HNTs-S2	530.2	458.9	517.2	515.3	168.9	0.049	0.33

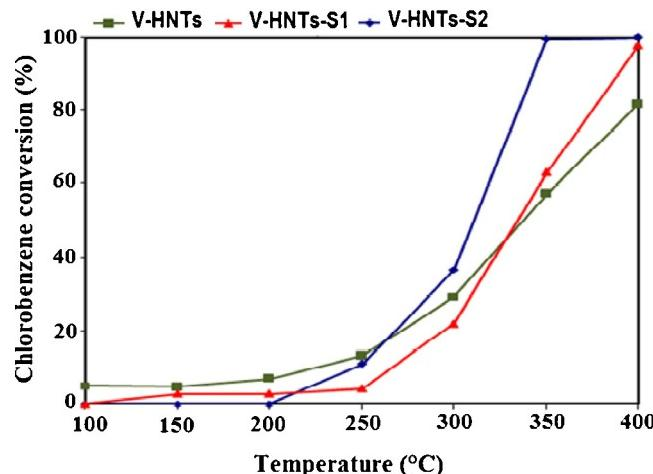


Fig. 9. Chlorobenzene conversion over vanadia supported catalysts.

of vanadia since the vanadium reduction peak maxima at 454 °C slightly shifted to higher temperatures (weak peaks at 528 and 520 °C for V-HNTs-S1 and V-HNTs-S2 catalysts, respectively). These observations suggest that the presence of SO_4^{2-} ions probably stabilize the vanadium in a higher oxidation state which might be beneficial for chlorobenzene oxidation [16,23]. Similarly, the presence of vanadium at the surface of sulfated catalysts enhances the reduction behavior of sulfate groups. Especially, the reducibility of sulfate was observed more important in the sulfated V/HNTs materials than non sulfated HNTs support. Indeed, TPR reduction peaks shifted toward lower temperatures (634 and 623 °C for V-HNTs-S1 and 536 °C for V-HNTs-S2). These observations highlight the existence of an electronic interaction between vanadium-Titanium and sulfates as described in Fig. 6. However, this interaction is more pronounced in the case of the 'in situ' elaborated sulfated V-catalyst.

Fig. 9 summarizes the chlorobenzene conversion of the catalysts in the range 100–400 °C. CO_2 is the main product. The carbon balance is completed with carbon monoxide, which is also produced especially at a relatively high temperature (from a few percent up to ca. 30%). No other partial oxidation products (chlorinated or not) are observed. Each temperature was maintained for 2 h and 30 min and iso-conversion was always observed. These observations hold for all catalysts.

The V/HNTs catalyst is virtually inactive for chlorobenzene conversion below 250 °C and exhibits an activity around 81% at 400 °C. The introduction of sulfates clearly leads to more active vanadia catalysts, with respect to V-HNTs. V-HNTs-S2 and V-HNTs-S1 sulfated catalysts reached indeed 100% and 97.5% of chlorobenzene conversion at 350 °C and 400 °C, respectively. These observations pointed out the beneficial role of sulfated hydrogenotitanate nanotubes as support. The enhancement of the catalytic activity of V-HNTs-S1 based catalysts in chlorobenzene oxidation at moderate temperature could be related to the structure of the active site. Based on DRIFTS results, the surface structure in the hydrogenotitanate nanotubes is the bridged bidentate form (Fig. 5) with H forming a Brønsted site ($\text{Ti}_2\text{SO}_4\text{H}$). The titanium electron deficiency in bridged bidentate form should be different compared to the

chelating bidentate. These observations suggest that the presence of bridged bidentate form probably stabilize the vanadium in a higher oxidation state as shown by $\text{H}_2\text{-TPR}$. In fact, sulfates on the surface of vanadia based catalysts significantly affect both the redox and the acidic properties of these materials as evidenced by $\text{H}_2\text{-TPR}$ and $\text{NH}_3\text{-TPD}$ experiments. This result corroborates with previous researches which showed that the interaction between sulfated titanium and vanadium species enhances the reducibility of VTiS materials and the reactivity of vanadium redox sites, leading to more active catalysts [12,16,52,60].

Moreover, it seems that the elaboration route of sulfated V-catalysts 'in situ' or 'ex situ' influences the environment of vanadium species. In particular, the 'in situ' way leads to a more efficient catalyst although vanadium is less exposed (XPS results). The explanation that we advance is that the beneficial effect of sulfation is further enhanced when the catalyst is prepared by the 'in situ' route as shown by $\text{NH}_3\text{-TPD}$ results. Also, the interaction between vanadium and sulfate groups was more pronounced in the case of V-HNTs-S2 as evidenced by $\text{H}_2\text{-TPR}$. These two effects seem to outweigh the loss of V species via the 'in situ' way.

4. Conclusion

We demonstrated the application of high surface area sulfated TiO_2 nanotubes (HNTs) as promising support for the V_2O_5 based materials. Sulfation of HNTs materials yields to the formation of bridged bidentate titanium and generates more acidic sites at the surface, which likely (i) govern the chlorobenzene oxidation and (ii) decreases the reducibility of vanadium leading to higher reactivity of redox sites and consequently to higher efficiency of the catalysts.

Acknowledgments

This work was done under the framework of bilateral collaboration between the Laboratoire de Chimie des Matériaux et Catalyse (LCMC) de la Faculté des Sciences de Tunis and l'Université Catholique de Louvain, Institute of Condensed Matter and Nanosciences (IMCN), Division «Solids, Molecules and Reactivity (MOST)». The LCMC of the University El-Manar and IMCN-MOST of the University Catholique de Louvain are greatly acknowledged.

References

- [1] J. Haber, Catal. Today 142 (2009) 100–113.
- [2] J. Jones, J.R.H. Ross, Catal. Today 35 (1997) 97.
- [3] S. Krishnamoorthy, J.A. Rivas, M.D. Amiridis, J. Catal. 193 (2000) 264–272.
- [4] I.E. Wachs, G. Deo, B.M. Weckhuysen, A. Andreini, M.A. Vuerman, M. Boer, M.D. Amiridis, J. Catal. 161 (1996) 211–221.
- [5] S. Krishnamoorthy, J.P. Baker, M.D. Amiridis, Catal. Today 40 (1998) 39–46.
- [6] S. Albonetti, S. Blasioli, R. Monelli, A. Bruno, J. Epoupa Mengou, S. Scirè, F. Trifirò, Appl. Catal. A: Gen. 341 (2008) 18–25.
- [7] S. Albonetti, J. Epoupa Mengou, F. Trifirò, Catal. Today 119 (2007) 295–300.
- [8] S. Albonetti, S. Blasioli, A. Bruno, J. Epoupa Mengou, F. Trifirò, Appl. Catal. B: Environ. 64 (2006) 1–8.
- [9] J. Lichtenberger, M. Amiridis, J. Catal. 223 (2004) 296–308.
- [10] M.A. Larrubia, G. Busca, Appl. Catal. B: Environ. 39 (2002) 343–352.
- [11] F. Bertinchamps, C. Grégoire, E.M. Gaaigneaux, Appl. Catal. B: Environ. 66 (2006) 1–9.
- [12] F. Bertinchamps, C. Grégoire, E.M. Gaaigneaux, Appl. Catal. B: Environ. 66 (2006) 10–22.

- [13] B. Schimmoeller, R. Delaigle, D.P. Debecker, E.M. Gaigneaux, *Catal. Today* 157 (2010) 198–203.
- [14] D.P. Debecker, R. Delaigle, K. Bouchmella, P. Eloy, E.M. Gaigneaux, P.H. Mutin, *Catal. Today* 157 (2010) 125–130.
- [15] C. Gannoun, R. Delaigle, P. Eloy, D.P. Debecker, A. Ghorbel, E.M. Gaigneaux, *Appl. Catal. A: Gen.* 447–448 (2012) 1–6.
- [16] C. Gannoun, R. Delaigle, P. Eloy, D.P. Debecker, A. Ghorbel, E.M. Gaigneaux, *Catal. Commun.* 15 (2011) 1–5.
- [17] T. Kasuga, M. Hiramatsu, A. Hoson, T. Sekino, K. Niihara, *Langmuir* 14 (1998) 3160–3163.
- [18] T. Kasuga, M. Hiramatsu, A. Hoson, T. Sekino, K. Niihara, *Adv. Mater.* 11 (1999) 1307–1311.
- [19] H. Kochkar, N. Lakhdhar, G. Berhault, M. Bausach, A. Ghorbel, *J. Phys. Chem. C* 113 (2009) 1672–1679.
- [20] H. Kochkar, A. Turki, L. Bergaoui, G. Berhault, A. Ghorbel, *J. Colloid Interface Sci.* 331 (2009) 27–31.
- [21] A. Turki, H. Kochkar, G. Berhault, A. Ghorbel, *Stud. Surf. Sci. Catal.* 175 (2010) 593–596.
- [22] D.V. Bavykin, A.A. Lapkin, P.K. Plucinski, L. Torrente-Murciano, J.M. Friedrich, F.C. Walsh, *Top. Catal.* 39 (2006) 151–160.
- [23] R. Delaigle, D.P. Debecker, F. Bertinchamps, E.M. Gaigneaux, *Top. Catal.* 52 (2009) 501–516.
- [24] H. Zhao, S. Bennici, J. Shen, A. Aurooux, *J. Mol. Catal. A* 309 (2009) 28–34.
- [25] W. Wang, O.K. Varghese, M. Paulose, C.A. Grimes, Q. Wang, E.C. Dickey, *J. Mater. Res.* 19 (2004) 417–422.
- [26] Q. Chen, L.-M. Peng, *Int. J. Nanotechnol.* 4 (2007) 44–65.
- [27] Q. Chen, G.H. Du, S. Zhang, L.-M. Peng, *Acta Crystallogr. B* 58 (2002) 587–593.
- [28] A. Nakahira, W. Kato, M. Tamai, T. Isshiki, K. Nishio, H. Aritani, *J. Mater. Sci.* 39 (2004) 4239–4245.
- [29] J. Yang, Z. Jin, X. Wang, W. Li, J. Zhang, S. Zhang, X. Guo, Z. Zhang, *Dalton Trans.* (2003) 3898–3901.
- [30] S. Mozia, E. Borowiak-Paleń, J. Przepiórski, B. Grzmil, T. Tsumura, M. Toyoda, J. Grzechulska-Damszel, A.W. Morawski, *J. Phys. Chem. Solids* 71 (2010) 263–272.
- [31] B. Vijayan, N.M. Dimitrijevic, T. Rajh, K. Gray, *J. Phys. Chem. C* 114 (2010) 12994–13002.
- [32] F. Maxim, P. Ferreira, P.M. Vilarinho, *J. Porous Mater.* 18 (2011) 37–45.
- [33] J. Huang, Y. Cao, M. Wang, C. Huang, Z. Deng, H. Tong, Z. Liu, *J. Phys. Chem. C* 114 (2010) 14748–14754.
- [34] C.K. Lee, C.C. Wang, M.D. Lyu, L.C. Juang, S.S. Liu, S.H. Hung, *J. Colloid Interface Sci.* 316 (2007) 562–569.
- [35] E. Morgado Jr., M.A.S. de Abreu, G.T. Moure, B.A. Marinkovic, P.M. Jardim, A.S. Araujo, *Chem. Mater.* 19 (2007) 665–676.
- [36] S.T. Myung, N. Takahashi, S. Komaba, C.S. Yoon, Y.K. Sun, K. Amine, H. Yashiro, *Adv. Funct. Mater.* 21 (2011) 3231–3241.
- [37] S. Zhang, W. Li, Z. Jin, J. Yang, J. Zhang, Z. Du, Z. Zhang, *J. Solid State Chem.* 177 (2004) 1365–1371.
- [38] A. Turki, H. Kochkar, C. Guillard, G. Berhault, A. Ghorbel, *Appl. Catal. B: Environ.* 134 (2013) 167–173.
- [39] G. Socrates, *Infrared Characteristic Group Frequencies second ed.* (1994) 168–169.
- [40] O. Saur, M. Bensitel, A.B. Mohammed Saad, J.C. Lavalley, C.P. Tripp, B.A. Morrow, *J. Catal.* 99 (1986) 104–110.
- [41] M.A. Fox, M.T. Dulay, *Chem. Rev.* 93 (1993) 341–357.
- [42] H. Zhao, S. Bennici, J. Shen, A. Aurooux, *J. Catal.* 272 (2010) 176–189.
- [43] T. Yamaguchi, *Appl. Catal.* 61 (1990) 1–25.
- [44] O. Saur, M. Bensitel, M. Saad, J.C. Lavalley, C.P. Tripp, B.A. Morrow, *J. Catal.* 99 (1986) 104.
- [45] P. Fornasiero, G. Baldacci, R. Di Monte, J. Kaspar, V. Sergio, G. Gubitosa, A. Ferrero, M. Graziani, *J. Catal.* 164 (1996) 173–183.
- [46] J.P. Nogier, M. Delamare, *Catal. Today* 20 (1994) 109–123.
- [47] V.I. Bukhtiyarov, *Catal. Today* 56 (2000) 403–414.
- [48] G. Silversmit, D. Depla, H. Poelman, G.B. Marin, R. De Gryse, *J. Electron Spectrosc. Relat. Phenom.* 135 (2004) 167–175.
- [49] B.M. Reddy, K.N. Rao, G.K. Reddy, A. Khan, S.-E. Park, *J. Phys. Chem. C* 111 (2007) 18751–18758.
- [50] B.M. Reddy, P. Bharali, P. Saikia, A. Khan, S. Loridan, M. Muhler, W. Grunert, *J. Phys. Chem. C* 111 (2007) 10478–10483.
- [51] J.P. Chen, R.T. Yang, *J. Catal.* 139 (1993) 277–288.
- [52] S.T. Choo, Y.G. Lee, I.-S. Nam, S.W. Ham, J.B. Lee, *Appl. Catal. A* 200 (2000) 177–188.
- [53] M.H. Kim, L.-S. Nam, Y.G. Kim, *J. Catal.* 179 (1998) 350–360.
- [54] L. Chmielarz, P. Kustrowski, M. Zbroja, W. Lasocha, R. Dziembaj, *Catal. Today* 90 (2004) 43–49.
- [55] J. Arfaoui, L. Khalfallah Boudali, A. Ghorbel, *Appl. Clay Sci.* 48 (2010) 171–178.
- [56] L. Baraket, A. Ghorbel, P. Grange, *Appl. Catal. B* 72 (2007) 37–43.
- [57] J. Arfaoui, L. Khalfallah Boudali, A. Ghorbel, G. Delahay, *Catal. Today* 142 (2009) 234–239.
- [58] H. Poelman, B.F. Sels, M. Olea, K. Eufinger, J.S. Paul, B. Moens, I. Sack, V. Balcaen, F. Bertinchamps, E.M. Gaigneaux, P.A. Jacobs, G.B. Marin, D. Poelman, R. De Gryse, *J. Catal.* 245 (2007) 156–172.
- [59] G.Y. Popova, T.V. Andrushkevich, E.V. Semionova, Y.A. Chesalov, L.S. Dovlitova, V.A. Rogov, V.N. Parmon, *J. Mol. Catal. A* 283 (2008) 146–152.
- [60] X. Gu, J. Ge, H. Zhang, A. Aurooux, J. Shen, *Thermochim. Acta* 451 (2006) 84–93.